BAU Journal - Science and Technology

Volume 3 | Issue 1
ISSN: 2706-784X

Article 2

December 2021

PHYSICAL AND MAGNETIC PROPERTIES OF NANOSIZED MN0.5NI0.5¬FE2-XPRXO4 PREPARED BY CO-PRECIPITATION METHOD

Douaa El-Said Bakeer
Post Graduate Student, Faculty of Science, Damanhour University, Eygpt, d_bakeer2010@yahoo.com

Khulud Habanjar
Doctor, Faculty of Science, Beirut Arab University, Lebanon, k.habanjar@bau.edu.lb

Ghassan Youness
Head of Chemistry Department and Professor of Physical Chemistry, Faculty of Science, Beirut Arab University, ghass@bau.edu.lb

Mohammad Abou Ghoush
Doctor, Faculty of Science, Beirut Arab University, Lebanon, mma284@student.bau.edu.lb

PHYSICAL AND MAGNETIC PROPERTIES OF NANOSIZED MN0.5NI0.5¬FE2-XPRXO4 PREPARED BY CO-PRECIPITATION METHOD

Abstract

Nanosized $Mn_{0.5}Ni_{0.5}Fe_{2-x}Pr_xO_4$, x=0.0, 0.02, 0.04, 0.06, 0.08, 0.1 and 0.15 are prepared by co-precipitation method at calcination temperature 650^oC for 4 hours. X-ray diffraction patterns show the presence of the cubic (Mn-Ni)- ferrite phase and anti-ferromagnetic a-Fe_2O_3. The variation in the lattice parameter "*a*" is due to the replacement of smaller radius ions Fe^{+3} by larger radius ions Pr^{+3}. Transmission electron micrographs indicate that the particles are spherical in shape. The moderately agglomerated particles are present due to the interaction between the magnetic nanoparticles. UV-visible optical (UV) and Fourier Transform Infrared (FTIR) spectroscopies show a significant change in the absorption bands as the Pr content increases. The calculated values of the optical band gap energies show an increase as the Pr content increases. This is due to the decrease of the particle size. From VSM analysis, it was found that the saturation magnetization (M_s) and the coercivity (H_c) are strongly dependent on Pr content. The results of M-H loop are interpreted in terms of the observed anti-ferromagnetic phase a-Fe_2O_3, phase core shell interaction and cation redistribution.

Keywords

(Mn-Ni)-ferrite nanoparticles, co-precipitation method, VSM

1. INTRODUCTION:

Magnetic nanoparticles have exhibit large attention owing to the unique magnetic properties derived from their nanosize and uniform size distribution [1]. Compared to their conventional bulk components, nanosized's small dimension at the grain boundaries is the main source responsible for its superior magnetic, electrical, dielectric and mechanical properties [2,3].

Spinels have been attractive to researches for continuous scientific interest and have been deeply investigated in materials science because of their superior physico-chemical properties [4]. Among spinel compounds, spinel ferrites (AB_2O_4, M= Ni, Mn,Zn, etc.) have received much research attention due to broad practical applications in several important technological fields such as ferrofluids, hyperthermia for cancer therapy, magnetic high-density information storages [5–7]. In normal spinels, all the A-sites (tetrahedral) are occupied by divalent transition metal ions while in inverse spinels, the divalent ions occupy B-sites (octahedral). The concentrations of ferrous, ferric and substituted metal ions and their distribution over tetrahedral and octahedral sites play a vital role in determining their magnetic and electrical properties [8].

Mn–Zn ferrite, as a soft magnetic material, is an important member of spinel family [9]. Many synthesis approaches have been employed to prepare nanosized spinel ferrite materials such as the sol-gel method [10], micelle and hydrothermal method [11], microemulsion method [12] and the co-precipitation method [13]. Among these methods, co-precipitation method turns to be the mostly used one to prepare nanocrystalline of a variety of materials due to its simplicity, low cost and its ability to control the grain sizes and their distribution [14]. Several researched were studied the effect of the rare earth elements substitution on the spinel ferrites [14-19]. The results showed a change in the grain size as well as an enhancement in the magnetic properties of ferrites due to substitution by different ions.

In the present work, the effect of partial substitution of Fe^{+3} ions by Pr^{+3} in structure, optical and magnetic properties of (Mn-Ni)-ferrite was investigated. For this purpose, samples of $Mn_{0.5}Ni_{0.5}Fe_{2-x}Pr_xO_4$ (x=0, 0.02, 0.04, 0.06, 0.08, 0.1, 0.15) were synthesized by co-precipitation method. The samples are characterized by X-ray powder diffraction (XRD), Transmission electron microscope (TEM) and Fourier transform infrared (FTIR). The optical and magnetic properties of the prepared samples are also examined by UV-vis spectroscopy and the vibrating sample magnetometer (VSM). The results show that the properties of (Mn-Ni)- ferrite are strongly affected by the concentration of Pr^{3+}.

2. EXPERIMENTS AND CHARACTERIZATION:

2.1 Preparation of Nano Powder

Nanosized samples of $Mn_{0.5}Ni_{0.5}Fe_{2-x}Pr_xO_4$, with x=0.0, 0.02, 0.04, 0.06, 0.08, 0.1 and 0.15, are prepared by co-precipitation method. The analytical grade chemical reagents are $MnCl_2.(4H_2O)$, $NiCl_2.(6H_2O)$, $FeCl_3.(6H_2O)$ and $PrCl_3.(7H_2O)$. Stoichiometric ratios are dissolved in distilled water and mixed using magnetic stirrer at 60 ºC. 4M NaOH solution is added drop by drop to the mixture with continuous magnetic stirring until the pH reaches 12.5. Then the solution is heated with continuous stirring at 60 ºC for 2 h. The formed precipitate is washed using distilled water to remove unwanted salt residues and are finally dried at 80 ºC for 24 h. Finally, the dried powder is calcined at 650 ºC for 4 h to improve the crystalline properties.

2.2 Characterization of the Samples

Samples of $Mn_{0.5}Ni_{0.5}Fe_{2-x}Pr_xO_4$ are characterized by XRD using Bruker D8 advance powder diffractometer with Cu-Kα radiation (λ = 1.54056 Å) in the range $4^\circ \leq 2\theta \leq 80^\circ$. The particle morphology is observed using Jeol transmission electron microscope JEM- 100CX, operated at 80 kV. Functional groups of the samples are studied via Fourier Transform Infrared Spectroscopy (FTIR) using Michelson interferometer. The optical band gap energy of the samples is calculated by using the UV-visible optical spectroscopy, in the range 200 nm and 700nm, obtained by V-670 NIR Spectrophotometer. The magnetic effect of manganese and iron doping on zinc oxide is analyzed by tracing room temperature magnetic hysteresis loops using vibrating sample magnetometers (VSM) Lakeshore 7410.

3. RESULTS AND DISCUSSION:

3.1 Structure and Morphology

XRD patterns of $Mn_{0.5}Ni_{0.5}Fe_{2-x}Pr_xO_4$ are shown in figure 1. Obviously, the diffraction peaks indicate the formation of cubic spinel structure of Mn-Ni ferrites [20,21] with space group Fd3m. Some additional peaks belong to anti-ferromagnetic material (α-Fe_2O_3) [22]. Hessien et al [23] and Hu et al [24] reported that the extra hematite phase, considered as an extra phase, may be completely dissolved and converted to ferrite phase at 1200^0C. It is clear that the relative concentration of hematite increases with the gradual increasing in Pr^{3+} concentration. The lattice constant a of spinel structure can be calculated for prominent peak (311) as follows:

$$a = d_{hkl}\sqrt{h^2 + k^2 + l^2} \qquad (1)$$

where d_{hkl} is the interplanar distance and (h, k, l) are the miller indices. Lattice constant values at different concentrations of Pr^{3+} are listed in Table 1. It is clear that the lattice parameter "a" slightly changes as the doping of Pr^{3+} increases, and this is attributed to the difference in ionic radii of Pr^{3+} (1.013 Å) and Fe^{3+} (0.64Å) [40]. Pr^{3+} ions are expected to enter into the octahedral sites in place of Fe^{3+} ions which could result in an internal stress to make the lattice distorted and an expansion of unit cell, resulting in the larger lattice constants [25, 26]. Similar results are reported [27, 28]. The average crystallite sizes of the samples are calculated from XRD using Debye- Scherer's formula

$$D = \frac{k\lambda}{\beta \cos\theta} \qquad (2)$$

where, D is the average crystallite size, λ is the X-ray wavelength, β is the full width at half maximum (FWHM), θ is Bragg angle and k is Scherrer constant equal to 0.9. As listed in table 1, the crystallite size gradually decreases for x>0.02 of Pr^{3+}. This may be due to larger bond of Pr^{3+} — O^{2-} as compared with Fe^{3+}— O^{2-} which requires more energy to make Pr ions enter into the lattice to complete crystallization and grow grains [29,30].

TEM micrographs of nanosized $Mn_{0.5}Ni_{0.5}Fe_{2-x}Pr_xO_4$, x = 0.0, 0.04, 0.1 and 0.15, are shown in Figures 2(a-d). The observed inhomogeneous crystalline structure is mainly due to the presence of secondary (α-Fe_2O_3) phase. It is clear that the particles are spherical in shape. Some moderately agglomerated particles are present due to the interaction between the magnetic nanoparticles. Moreover, the average grain size is decreased with increasing Pr^{3+} concentration, as listed in Table 1. This result is consistent with XRD results. The particle sizes estimated from TEM images are rather smaller than those estimated from XRD spectra, this is probably due to the fact that the samples for TEM measurements are prepared from reaction solution and not from powder. At this point, aging conditions play a decisive role in the particle sizes. Particle sizes in reaction solution are susceptible to aging effects which in turn may result in higher band gap energy [15]. Thus, the aging in reaction solution is one of the main effects responsible for deviation in sizes measured by XRD and TEM.

3.2 FTIR Analysis:

FTIR spectra of nanosized $Mn_{0.5}Ni_{0.5}Fe_{2-x}Pr_xO_4$ are shown in figure 3. The vibrations in a crystal lattice are usually observed in the range of 300–700 cm^{-1}[31]. The highest one, ν_1, is generally observed at 590 cm^{-1} which caused by the stretching vibrations of tetrahedral metal–oxygen bond, whereas the lowest band, ν_2, is usually observed at 445 cm^{-1} which is assigned to octahedral metal stretching. It is seen from Figure 3, the high frequency band ~600 cm^{-1} peak is the stretching vibration of tetrahedral metal oxygen bond between Fe^{3+} and O^{2-} that commonly features in the ferrites [32]. As it is seen in Figure 3, the Fe–O stretching vibration has a little shifting to higher wavenumber. Similarly shifting in the band positions is reported in the literature [33,34]. This shift is due to the disorder occurring between Fe^{3+} and O^{2-} bond kind of substituting Pr^{3+} atoms [33].

3.3 UV-Spectroscopy

Optical investigation of nanosized $Mn_{0.5}Ni_{0.5}Fe_{2-x}Pr_xO_4$, in the wavelength range of 200 to 700nm, is shown in figure 4. The sharp peak at 272 nm and 372 nm in the UV–visible spectra indicates that the colloids are well dispersed. The absorption peak of the doped (Mn-Ni)-ferrite samples showed a blue shift towards a smaller wavelength. This shift might be due to surface effects, change in the crystallite size, morphology or an indication that the electronic structure of undoped (Mn-Ni) ferrites is altered by Pr doping [35]. The optical band gap energy of nanosized $Mn_{0.5}Ni_{0.5}Fe_{2-x}Pr_xO_4$ for direct band gap is calculated by using Tauc's relation:

$$(\alpha h\upsilon)^n = A(h\upsilon - E_g) \qquad (3)$$

where E_g is the optical band gap energy and υ is the frequency of the incident photon, n is either 2 for a direct band gap material or 2/3 for indirect band gap material, (hυ) is incident photon energy. The Tauc's optical gap is determined by plotting $(\alpha h\upsilon)^2$ over a limited range of photon energies hυ and the extrapolation of the linear part of the curve $(\alpha h\upsilon)^2=0$, as shown in the figure 5. The absorption coefficient (α) has been calculating using the measured absorbance ($\alpha = 4\pi k'/\lambda$) with k' being the absorption index or absorbance. The obtained values of the optical band gap energies (E_g) are listed in Table 2. E_g shows an increase as the Pr content increases. This could be due to the decrease of the particle size and the decrease of density of localized state in the conduction band [36]. This can be explained on the basis of Bras' effective mass model [37] according to which the measured band gap, E_g can be expressed as a function of particle size as:

$$E_g = E_g^{\,bulk} + \frac{h^2\pi^2}{2er^2}\left(\frac{1}{m_e} + \frac{1}{m_h}\right) - \frac{1.8e^2}{4\pi\varepsilon\varepsilon_{0r}} \qquad (4)$$

where r is the particle size, $E_g^{\,bulk}$ is the bulk energy gap, m_e is the effective mass of the electron, m_h is the effective mass of the holes. ε and ε_0 are the relative permittivity and free space permittivity, respectively. $\hbar$ is the Planck's constant divided by 2π and e is the charge on electron.

3.4 Magnetic Measurements:

The magnetic measurements are carried out by using M-H hysteresis loops at room temperature and are shown in Figure 6. From these curves, saturation magnetization (M_s), remanence magnetization (M_r), the corecivity H_c and magnetic moment μ_m are determined and the values of these quantities are listed in Table 3. The magnetic moment (μ_m) per unit formula in Bohr magneton is calculated from saturation magnetization by using the following formula:

$$\mu_m = (M_w \times M_s)/5585 \qquad (5)$$

where, μ_m is the magnetic moment and M_w is the Moleculer weight. Obviously, it is clear that all samples are ferrimagnetic in nature. As seen from table 3, as the content of Pr^{3+} increases from 0.0 to 0.06, M_s increases from 22.528 emu/g to 49.7 emu/g. Upon further increases in Pr^{3+} content, M_s decreases to reach 17.018 emu/g. The increase in M_s till x = 0.06 may be because Fe^{3+} ions do not occupy all octahedral sites and also a small fraction can occupy tetrahedral sites, i.e., the inversity increases with Pr substitution which prefers occupying octahedral sites and hence the magnetic moment (μ_m) is enhanced also [30] The decrease in the M_s with increase in the Pr^{3+} content is very likely related to decrease in the particle size. This size dependent effect has been well established in magnetite nanoparticles where it was interpreted in terms of the presence of magnetic dead layer on the surface of a nanoparticle [38]. Also, the decrease in M_s can be attributed to the formation of the anti-ferro magnetic material (α-Fe_2O_3) or the cation redistribution between tetrahedral (A) and octahedral (B) sites.[39]. Moreover, the coercivity H_c and the M_r also depends on particle size [15].

4. CONCLUSION:

Nanosized samples $Mn_{0.5}Ni_{0.5}Fe_{2-x}Pr_xO_4$ were successfully synthesized by co-precipitation method. XRD analysis patterns showed the presence of the cubic ferrite phase as well as hematite as impurity phase (α-Fe_2O_3). The lattice constant increased slightly as the concentration of Pr^{3+} increased. This is probably due to the replacement of smaller radius ions $Fe^{3+}$by larger radius ions Pr^{3+}. Moreover, the crystallite size gradually decreased as the concentration of Pr increased. FTIR analysis showed two absorption peaks in the range of 400-600cm^{-1} characterizing the spinel ferrites. The optical band gap energy was found to increase with the increase of Pr content. This was attributed to the decrease of the particle size and the decrease of density of localized state in the conduction band. The magnetic study manifested the ferrimagnetic behavior of the prepared samples. The magnetic parameters were strongly affected by the concentration of Pr.

5. ACKNOWLEDGEMENTS

This work was done in cooperation between Beirut Arab University, American University of Beirut, Alexandria University and Lebanese Atomic Energy Commission.

REFERENCES:

- J.G. Li, X.D. Sun, Acta Mater. 48 (2000) 3103.
- Skandan, G., Hahn, H., Roddy, M., & Cannon, W. R. (1994). Ultrafine-grained dense monoclinic and tetragonal zirconia. *Journal of the American Ceramic Society*, *77*(7), 1706-1710.
- Giri, J., Sriharsha, T., Asthana, S., Rao, T. K. G., Nigam, A. K., & Bahadur, D. (2005). Synthesis of capped nanosized Mn1− xZnxFe2O4 (0⩽ x⩽ 0.8) by microwave refluxing for bio-medical applications. *Journal of magnetism and magnetic materials*, *293*(1), 55-61.
- Souza, L. K. C. D., & Zamian, J. R. (2009). GNDR Filho, LEB Soledade, IMGD Santos, AG Souza, T. Scheller, RS Angélica, CEFD Costa. *Dyes Pigm*, *81*, 187.
- Amici, J., Celasco, E., Allia, P., Tiberto, P., & Sangermano, M. (2011). Poly (ethylene glycol)-Coated Magnetite Nanoparticles: Preparation and Characterization. *Macromolecular Chemistry and Physics*, *212*(4), 411-416.
- Köseoğlu, Y., Bay, M., Tan, M., Baykal, A., Sözeri, H., Topkaya, R., & Akdoğan, N. (2011). Magnetic and dielectric properties of Mn 0.2 Ni 0.8 Fe 2 O 4 nanoparticles synthesized by PEG-assisted hydrothermal method. *Journal of Nanoparticle Research*, *13*(5), 2235-2244.
- Abareshi, M., Goharshadi, E. K., Zebarjad, S. M., Fadafan, H. K., & Youssefi, A. (2010). Fabrication, characterization and measurement of thermal conductivity of Fe3O4 nanofluids. *Journal of Magnetism and Magnetic Materials*, *322*(24), 3895-3901.
- Hussain, A., Abbas, T., & Niazi, S. B. (2013). Preparation of Ni1− xMnxFe2O4 ferrites by sol–gel method and study of their cation distribution. *Ceramics International*, *39*(2), 1221-1225.
- Sugimoto, M. (1999). The past, present, and future of ferrites. *Journal of the American Ceramic Society*, *82*(2), 269-280.
- Chander, S., Srivastava, B. K., & Krishnamurthy, A. (2004). Magnetic behaviour of nano-particles of Ni 0.5 Co 0.5 Fe 2 O 4 prepared using two different routes.
- Liu, X. M., Fu, S. Y., & Huang, C. J. (2004). Nanostructure and magnetic properties of NiFe2O4 in the silica matrix prepared by sol-gel technique. *J Magn Magn Mater*, *281*(2-3), 234-239.
- Wang, H. W., & Kung, S. C. (2004). Crystallization of nanosized Ni–Zn ferrite powders prepared by hydrothermal method. *Journal of Magnetism and Magnetic Materials*, *270*(1-2), 230-236.
- Bonini, M., Wiedenmann, A., & Baglioni, P. (2004). Synthesis and characterization of surfactant and silica-coated cobalt ferrite nanoparticles. *Physica A: Statistical Mechanics and its Applications*, *339*(1-2), 86-91.
- Bakeer, D. E. S., Abou-Aly, A. I., Mohammed, N. H., Awad, R., & Hasebbo, M. (2017). Characterization and Magnetic properties of nanoferrite ZnFe 2− x La x O 4 prepared by co-precipitation method. *Journal of Superconductivity and Novel Magnetism*, *30*(4), 893-902.
- Bitar, Z., Isber, S., Noureddine, S., Bakeer, D. E. S., & Awad, R. (2016). Synthesis, Characterization, Optical Properties, and Electron Paramagnetic Resonance for Nano.
- A.I.Ali, M.A.Ahmed, N.Okasha, M.Hammam, J.Y. Sonf,. J. Materr. Res. Technol. 2 (4) (2013) 356.

- Dixit, G., Singh, J. P., Srivastava, R. C., & Agrawal, H. M. (2012). Magnetic resonance study of Ce and Gd doped NiFe2O4 nanoparticles. *Journal of Magnetism and Magnetic Materials*, *324*(4), 479-483.
- Talebi, R., Nasiri, M., & Rahnamaeiyan, S. (2016). Synthesis, characterization and optical properties of lanthanum doped zinc ferrite nanoparticles prepared by sol–gel method. *Journal of Materials Science: Materials in Electronics*, *27*(2), 1500-1506.
- Kumar, P., Sharma, S. K., Knobel, M., Chand, J., & Singh, M. (2011). Investigations of lanthanum doping on magnetic properties of nano cobalt ferrites. *Journal of electroceramics*, *27*(2), 51-55.
- Q. M. Wei, J.B. Li, Y-jun. Chen, Y-sheng Han, Materials Chemistry and Physics 74 (2002) 340.
- P. Raju , S. R. Murthy, Appl Nanosci 3 (2013) 469.
- Jayaprakash, R., Seehra, M. S., Prakash, T., & Kumar, S. (2013). Effect of α-Fe2O3 phase on structural, magnetic and dielectric properties of Mn–Zn ferrite nanoparticles. *Journal of physics and chemistry of solids*, *74*(7), 943-949.
- Hessien, M. M., Rashad, M. M., El-Barawy, K., & Ibrahim, I. A. (2008). Influence of manganese substitution and annealing temperature on the formation, microstructure and magnetic properties of Mn–Zn ferrites. *Journal of Magnetism and Magnetic Materials*, *320*(9), 1615-1621.
- Hu, P., Yang, H. B., Pan, D. A., Wang, H., Tian, J. J., Zhang, S. G., ... & Volinsky, A. A. (2010). Heat treatment effects on microstructure and magnetic properties of Mn–Zn ferrite powders. *Journal of Magnetism and Magnetic Materials*, *322*(1), 173-177.
- Ishaque, M., Islam, M. U., Khan, M. A., Rahman, I. Z., Genson, A., & Hampshire, S. (2010). Structural, electrical and dielectric properties of yttrium substituted nickel ferrites. *Physica B: Condensed Matter*, *405*(6), 1532-1540.
- Rao, A. D. P., Ramesh, B., Rao, P. R. M., & Raju, S. B. (1999). Magnetic and microstructural properties of Sn/Nb substituted Mn–Zn ferrites. *Journal of alloys and compounds*, *282*(1-2), 268-273.
- [27] V. Nachbaura, G. Tauvel, T. Verdierb, M. Jeana, J. Juraszekb, D. Houvet, J. Alloys Compd. 473 (2009) 303.
- Stewart, S. J., Figueroa, S. J. A., López, J. R., Marchetti, S. G., Bengoa, J. F., Prado, R. J., & Requejo, F. G. (2007). Cationic exchange in nanosized Zn Fe 2 O 4 spinel revealed by experimental and simulated near-edge absorption structure. *Physical Review B*, *75*(7), 073408.
- A.Watcharapasorn, S. Jiansirisomboon, Ceramics Internationals 34 (2008) 769
- Tholkappiyan, R., & Vishista, K. (2014). Influence of lanthanum on the optomagnetic properties of zinc ferrite prepared by combustion method. *Physica B: Condensed Matter*, *448*, 177-183.
- Khosravi, I., Yazdanbakhsh, M., Goharshadi, E. K., & Youssefi, A. (2011). Preparation of nanospinels NiMnxFe2− xO4 using sol–gel method and their applications on removal of azo dye from aqueous solutions. *Materials Chemistry and Physics*, *130*(3), 1156-1161.
- Chhantbar, M. C., Trivedi, U. N., Tanna, P. V., Shah, H. J., Vara, R. P., Joshi, H. H., & Modi, K. B. (2004). Infrared spectral studies of Zn-substituted CuFeCrO4 spinel ferrite system.
- Shinde, T. J., Gadkari, A. B., & Vasambekar, P. N. (2012). Influence of Nd3+ substitution on structural, electrical and magnetic properties of nanocrystalline nickel ferrites. *Journal of Alloys and Compounds*, *513*, 80-85.
- Hemeda, O. M., Barakat, M. M., & HEMEDA, D. M. (2004). Structural, electrical and spectral studies on double rare-earth orthoferrites La_ {1-x} Nd_xFeO_3. *Turkish Journal of Physics*, *27*(6), 537-550.
- Azam, A., Ahmed, A. S., Habib, S. S., & Naqvi, A. H. (2012). Effect of Mn doping on the structural and optical properties of SnO2 nanoparticles. *Journal of Alloys and Compounds*, *523*, 83-87.
- P. Chand, A. Gaur, As.Kumar, International Journal of Chemical, Molecular, Nuclear, Materials and Metallurgical Engineering 8 (12) (2014) 1321.
- Azim, M., Chaudhry, M. A., Amin, N., Arshad, M. I., Islam, M. U., Nosheen, S., ... & Mustafa, G. (2016). Structural And Optical Properties Of Cr-Substituted Co-Ferrite Synthesis By Coprecipitation Method. *Digest Journal Of Nanomaterials And Biostructures*, *11*(3), 953-962.
- P. Dutta, S. Pal, M.S. Seehra, N. Shah, G.P. Huffman, J. Appl. Phys. 105 (2009) 07B501.
- E. Kumar, R. Jayaprakash, M. Seehra, S. Kumar, "Effect of α-Fe_2O_3 phase on structural, magnetic and dielectric properties of Mn–Zn ferrite nanoparticles", *Journal of Physics and Chemistry of Solids* 74 (2013) 943.

– M. T. Farid, I. Ahmad, S. Aman, "Characterization of nickel-based spinel ferrites with small substitution of praseodymium" *Journal of the Chemical Society of Pakistan* 35(3) (2013) 793.

Figures Captions:

Figure 1: XRD patterns for nanosized $Mn_{0.5}Ni_{0.5}Fe_{2-x}Pr_xO_4$ samples.
Figure 2: TEM images of nanosized $Mn_{0.5}Ni_{0.5}Fe_{2-x}Pr_xO_4$ samples:
(a) x = 0.0, (b) x= 0.04, (c) x= 0.1 and (d) x= 0.15.
Figure 3: FTIR spectra for nanosized $Mn_{0.5}Ni_{0.5}Fe_{2-x}Pr_xO_4$ samples annealed at 650 ºC.
Figure 4: The UV spectra of nanosized $Mn_{0.5}Ni_{0.5}Fe_{2-x}Pr_xO_4$ samples.

Figure 5: Photoresponse versus photon energy curves for the determination of the optical band gap energy of nanosized $Mn_{0.5}Ni_{0.5}Fe_{1.96}Pr_{0.04}O_4$ samples.
Figure 6: (M–H) curves of nanosized $Mn_{0.5}Ni_{0.5}Fe_{2-x}Pr_xO_4$ samples.

Table 1: lattice parameter *a*, crystallite size *D* using Sherrer equation (max peak) and TEM of $Mn_{0.5}Ni_{0.5}Fe_{2-x}Pr_xO_4$ samples

x	a (Å)	Average crystallite size *D* (nm)	
		XRD	TEM
0.00	8.359	34.42	11.24
0.02	8.335	35.33	9.97
0.04	8.358	19.88	8.30
0.06	8.343	14.62	8.07
0.08	8.334	17.25	6.53
0.10	8.347	18.13	4.86
0.15	8.376	16.85	5.47

Table 2: The optical band gap energy of nanosized $Mn_{0.5}Ni_{0.5}Fe_{2-x}Pr_xO_4$ samples

x	E_g (eV)
0.00	3.010
0.02	3.015
0.04	3.033
0.06	3.053
0.08	3.051
0.10	3.060
0.15	3.070

Table 3: Variation of saturation magnetization (M_s), remanence magnetization (M_r) , the corecivity (H_c) and magnetic moment μ_m for nanosized $Mn_{0.5}Ni_{0.5}Fe_{2-x}Pr_xO_4$

x	M_s (emu/g)	M_r (emu/g)	H_c (Oe)	μ_m
0.00	22.528	2.967	135.29	0.939
0.02	20.496	0.321	20.229	0.859
0.04	31.121	0.178	7.495	1.315
0.06	49.710	0.229	6.083	2.115
0.08	17.448	0.226	17.179	0.748
0.10	14.090	1.154	109.36	0.608
0.15	17.018	0.855	63.595	0.747

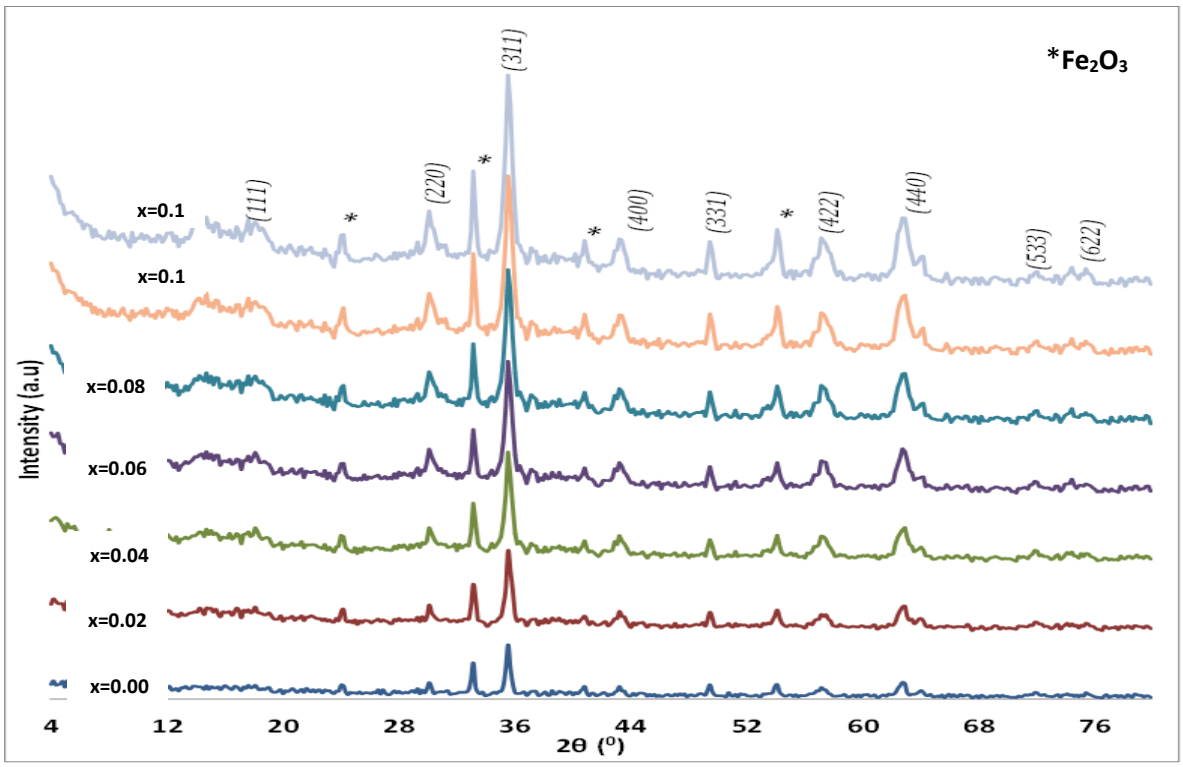
*Fe2O3
(111)
(220)
(311)
(400)
(331)
(422)
(440)
(533)
(622)
x=0.1
x=0.1
x=0.08
x=0.06
x=0.04
x=0.02
x=0.00
Intensity (a.u)
4
12
20
28
36
44
52
60
68
76
2θ (°)

Fig.1

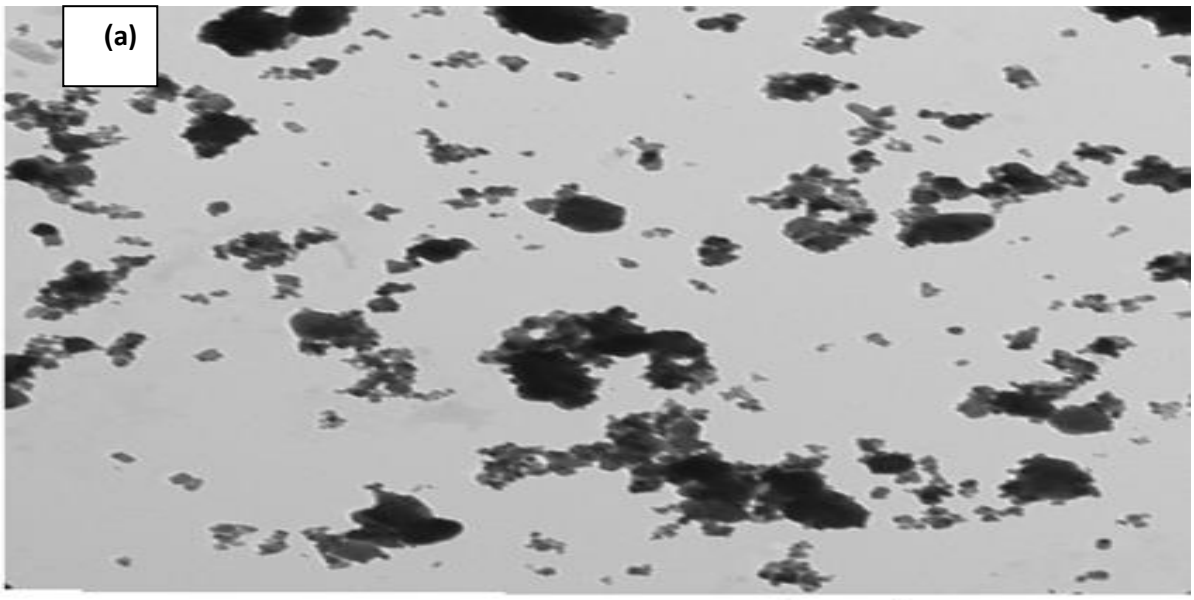
(a)
100 nm

Fig.2 (a)

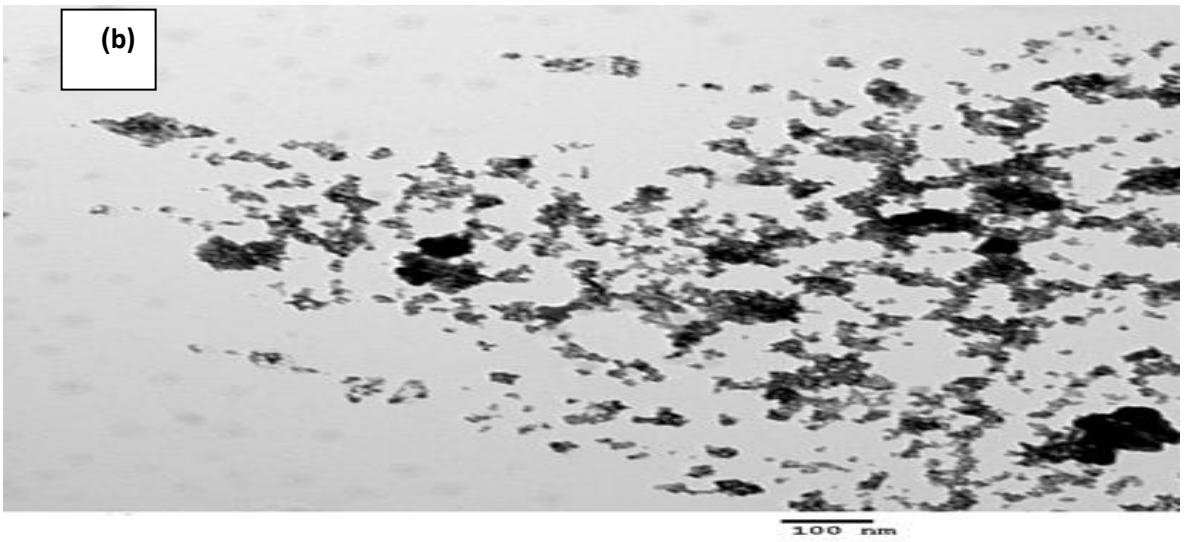

Fig.2 (b)

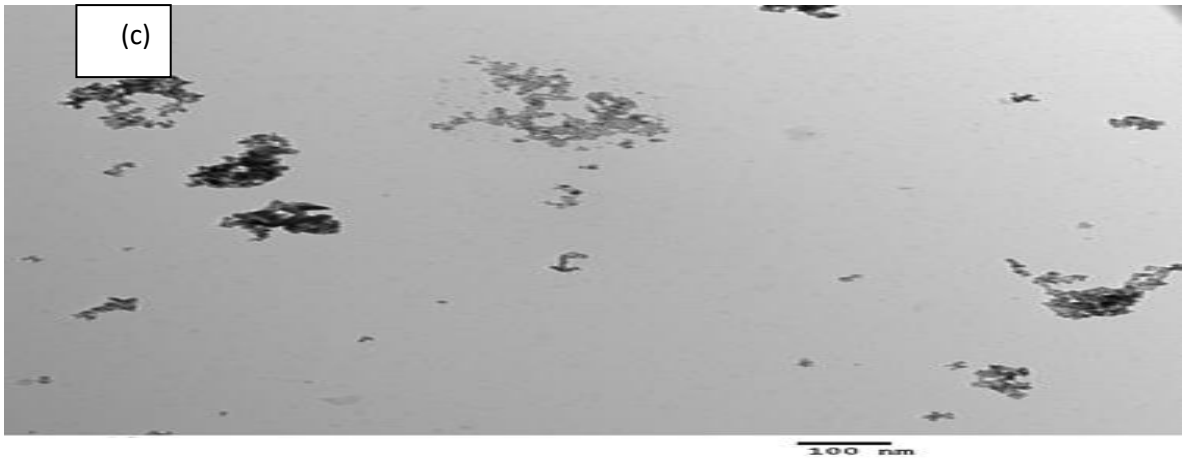

Fig. 2(c)

Fig. 2(d)

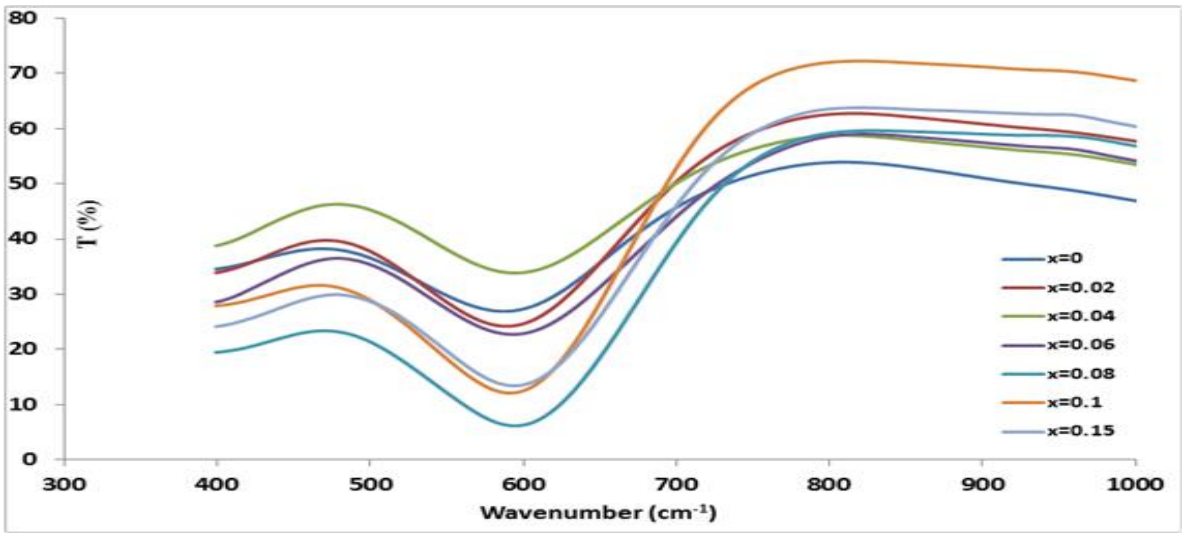

Fig.3

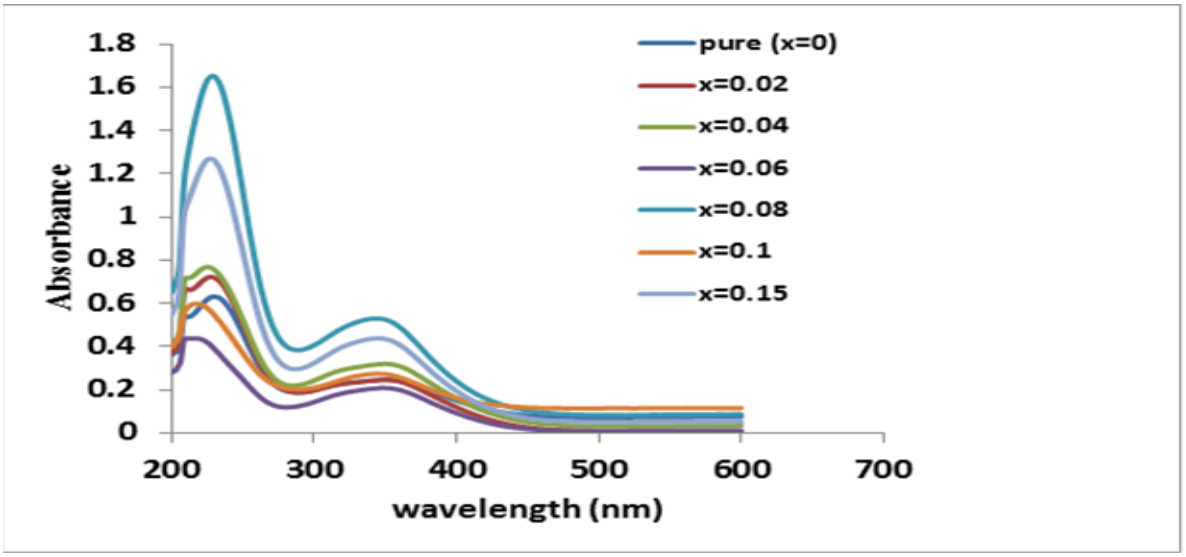

Fig.4:

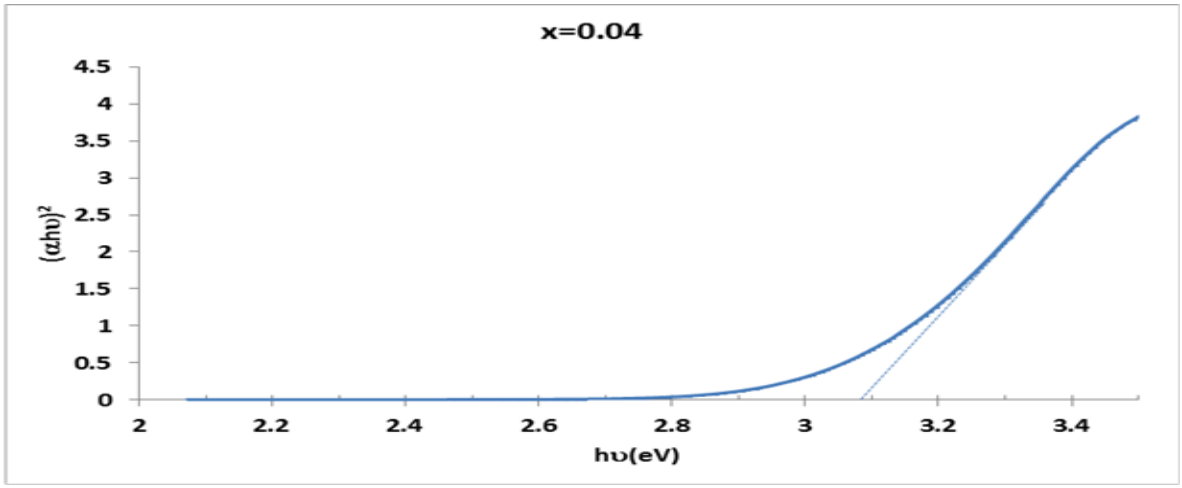

Fig.5

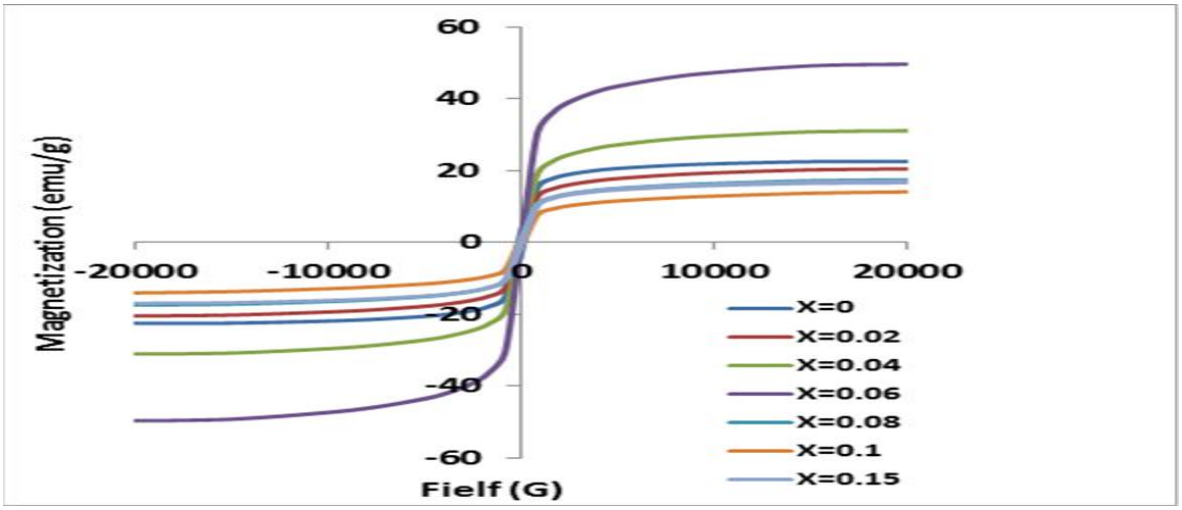
60
40
20
0
-20
-40
-60
-20000
-10000
0
10000
20000
Magnetization (emu/g)
Fielf (G)
X=0
X=0.02
X=0.04
X=0.06
X=0.08
X=0.1
X=0.15

Fig.6